

The semi-controlled reentry: development of a simulator and feasibility study

Anthea Evelina Comellini¹, Brice Dellandrea², Gautier Durand³, Pierluigi Di Lizia⁴

In this paper the assumptions underlying the implementation of a simulator for the propagation of very low altitude orbits, whose major aim is to provide a tool to study the feasibility of the semi-controlled re-entry, will be discussed. Then a semi-controlled reentry strategy based on electric propulsion will be defined and its feasibility in terms of maneuver duration, power balance, thermal limits, controllability and compliance with Space Debris Mitigation requirements will be studied. In this regard it will be explained how to interface the simulator with the already existing software for the analysis of satellites fragmentation and the assessment of fatality risk.

1. Introduction

Safeguarding Earth's orbital environment has recently gained a real attention: a report from the Inter-Agency Space Debris Coordination Committee (IADC) (1), states that the debris situation in low Earth orbit (LEO) may be reaching a catastrophic tipping point. A scenario where the density of objects in LEO is high enough that collisions between objects will cause a cascade of collisions, with each collision generating space debris thereby increasing the likelihood of further collisions (Kessler Syndrome), would prevent the use of any LEO. To face this environment challenge, the European Space Agency (ESA) has set up the Cleanspace initiative, which goes in two complementary directions: the Space Debris Remediation, which aims at reducing the number of existing debris, and the Space Debris Mitigation (SDM) that sets the requirements to protect LEO region. To comply with SDM requirements, LEO satellites have to be deorbited within 25 years or transferred into a high enough graveyard orbit, beyond the protected region. Moreover, in the case of a re-entry, total casualty risk has to be taken into account and kept below 10^{-4} .

Up to now satellites have been deorbited only through uncontrolled reentry: perigee is lowered down to an altitude where atmospheric drag causes the reentry within 25 years. The maneuver can be performed with any kind of propulsion but there is no way of controlling the epoch and the zone of impact. Only small satellites, which are likely to completely burn up during the reentry, can be deorbited in this way due to the fatality risk constraint. Satellite heavier than 700 kg can satisfy this constraint by performing a controlled reentry, which allows targeting a precise uninhabited area. This strategy requires a relatively high level of thrust, therefore chemical propulsion, which yields a larger amount of boarded propellant and higher launching cost. While uncontrolled reentry is unrealizable for heavy satellites, controlled reentry can be too much expensive. In order to merge the advantages coming from the exploitation of atmospheric drag and electric propulsion and the possibility of managing impact footprint and therefore fatality risk, a new approach was recently proposed: the semi-controlled re-entry. Semi-controlled reentry is not based on a final deorbiting manoeuvre executed to target precisely the location where the debris will fall on ground, but rather relies on controlling the satellite orbit down to a low altitude that enables the prediction of the debris footprint on ground with sufficient accuracy (1-2 ground-tracks), thus enabling a reduction of casualty risk through orbit phasing.

Figure 1 shows a schematic representation of this kind of strategy applied to a circular orbit, as suggested by the Centre National d'Etudes Spatiales (CNES). An initial controlled phase uses apogee boosts to slowly lower perigee altitude. Starting from a certain perigee altitude the atmospheric drag will significantly perturb the orbital motion, causing apogee lowering. As perigee keeps decreasing, aerodynamic perturbations will become more and more aggressive and will exceed Attitude and Orbital Control System (AOCS) capabilities. From this moment on, the propelled and controlled phase ends and the driving factor will be atmospheric drag: a rapid circularization process starts. During this phase, that is called decay phase and according to CNES should not be longer than 2 days, the satellite is completely subjected to aerodynamic perturbations and it can therefore drift away from its nominal orbit. As the satellite reaches an altitude between 80-90 km, it tends to break into fragments that can eventually reach the ground. Even if it is possible to predict with a certain confidence the ground-tracks of the satellite, the uncertainties deriving from the decay phase make it impossible to know the position of the impact footprint on the last ground-track. The compliance with SDM requirements is obtained by finding the proper phasing in order to have a final ground-track that avoids the most inhabited areas. The study will be divided in two

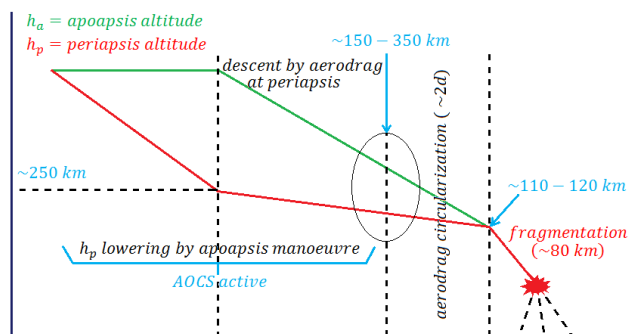


Figure 1: Semi-controlled reentry strategy

parts: the first part focuses on the development of a simulator to accurately describe the satellites dynamics during the reentry phase; the second part adopts the developed simulator in a study case.

¹Double degree graduated. Home University: Politecnico di Milano. Host University: ISAE Supaero

²Internship supervisor, head of Satellite Platforms R&D Service, Thales Alenia Space

³Internship supervisor, Satellite Platforms R&D Service, Thales Alenia Space

⁴MSc thesis advisor, Politecnico di Milano, Dipartimento di Scienze e Tecnologie Aerospaziali

2. LEO regime dynamics simulator

The first part of this work addresses the development of a simulator which could allow the user to perform a feasibility study of semi-controlled reentry, in terms of duration of the maneuver, power balance, thermal limits, controllability and compliance with SDM requirements. The simulator has been implemented by introducing a series of modifications and customizations to an already existing one that was built for the scenario of a Mars sample return mission. In this section the main features of the simulator will be briefly discussed, drawing the attention on the blocks purposely developed for this work, such as the atmospheric and aerodynamic blocks which have a direct impact on S/C controllability.

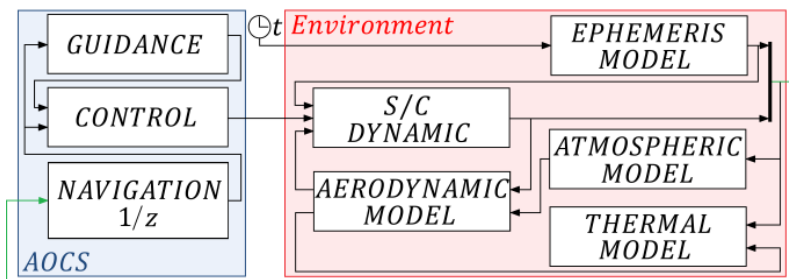


Figure 2: Simulink plan of the simulator

As shown in Fig. 2, the simulator is divided in two main blocks: the AOCS block and the Environment block. The outputs of the AOCS block are the inputs of the Environment block, while the outputs of the Environment block are the inputs of the AOCS. In the AOCS block the Navigation, Guidance and Control sections can be found. The dynamics of the sensors, the data processing and the estimation of the variables used by the guidance and the

control are not modeled in this work. Spacecraft position and velocity, the attitude quaternion and the angular rates, as well as reaction wheels rates and Sun-S/C position are computed in the Environment block and used in the AOCS block, passing only through a unit delay in the navigation block, which means that no estimation error is taken into account. Guidance algorithms can change with respect to each particular scenario (f.i. aero-stable attitude during perigee passage, sun pointing, etc). The controller is a classical PID controller capable of handling large attitude error angles, which is especially useful at the beginning-end of atmospheric passages. For such large errors, the control slews the satellite at a constant rate.

The Environment block contains all the blocks that compute environmental conditions (everything that can be considered extern with respect to the satellite system) and the blocks that compute the state of the satellite (mainly dynamics and thermal) due to the environmental inputs acting on it. The translational dynamics is propagated by Gauss perturbation equations written in a form robust towards small inclinations and eccentricities. Attitude dynamics is based on a rigid body model and takes into account also reaction wheels dynamics.

The inertial reference frame chosen for the simulator is the J2000 Earth centered reference frame. Time is measured in MJD2000. The mean orbital parameters of Earth orbit in J2000 are kept constants for the whole duration of the simulation. Within environmental block Ephemeris Model can be found. It computes the position of Sun with respect to the inertial reference system (Earth centered mean equatorial r.f) and the attitude of Earth with respect to its rotation axis. This makes it possible to compute the position of the S/C in terms of latitude and longitude, providing the inputs needed by the Atmospheric model.

The modelisation of the eclipse is simplified (cylindric model): the zone of shadow is a cylinder having radius equal to Earth radius and axis parallel to Earth-Sun vector oriented in the opposite direction. Eclipse is therefore considered as an on-off status (i.e., penumbra regions are not considered).

2.1 Atmospheric model

The atmospheric model used in the simulator is the *NRLMSISE-00* suggested by the European Cooperation for Space Standardization (ECSS) in (2). The Atmosphere Model block implements the mathematical representation of the 2001 United States Naval Research Laboratory Mass Spectrometer and Incoherent Scatter Radar Exosphere (NRLMSISE-00) of the MSIS[®] class mode. This is an empirical model based on atmospheric composition data from instrumented satellites and temperatures from ground-based radar. The covered altitudes go from ground to 1000 km, which is the lower exosphere. The block receives as input the position of the satellite expressed in latitude, longitude and altitude, and the date. Its outputs are the air temperature T , the mass density of the air ρ , and the number density nd_i (which is the number of molecule of species i contained in the unit volume V) of each species composing the atmosphere. The considered species are H, He, N, O, N_2, O_2 and Ar . In addition to these standard species the model adds a new specie, the so called “anomalous oxygen”, which is an ionized atom of oxygen (O^+) believed to be present in Earth's exosphere above 500 km near the poles during their respective summers. This additional component augments the mainly hydrogen and helium exosphere and explains the unexpectedly high drag forces on satellites passing near the poles in their summers.

Atmosphere temperature and mass density are not enough to fully determine the thermodynamics properties of the airflow needed by the simulator. The computation of aerodynamic coefficients needs both the Mach number M and the air heat capacity ratio γ . For M computation the speed of sound c is needed and, recalling the formula $c = \sqrt{\gamma R_{air} T}$, it can be noticed that also the specific gas constant of air R_{air} is needed. Moreover the computation of the Knudsen number K_n (see section 2.2) requires the computation of the total air static pressure P . In order to obtain these thermodynamic variables, gas mixture properties will be used. If the number density is divided by the Avogadro constant ($N_a = 6,022 \cdot 10^{23}$, number of molecules in a mole), the number of moles of species i contained in the unit volume (n_i/V) will be obtained. Dalton law for gas mixture states that the total pressure P of the mixture is the summation of the partial pressure P_i of the different species. Reminding the ideal gas state equation ($PV = nRT$, where $R = 8,314 \frac{J}{K \cdot mol}$), it is possible to write:

$$P = \sum_i P_i = \sum_i \frac{n_i}{V} R T = R T \sum_i \frac{nd_i}{N_a} = \frac{RT}{N_a} \sum_i nd_i \quad (1)$$

The number density and the temperature given by the model therefore allow to directly compute the gas pressure. Once that P is determined, air mass density ρ can be used to compute the specific air constant R_{air} . In fact state equation can also be written as:

$$P = \rho R_{air} T \longrightarrow R_{air} = \frac{P}{\rho T} \quad (2)$$

The computation of γ requires a longer process. Reminding Mayer's law, for a generic mixture, it is possible to write:

$$\begin{cases} C_{p_{mix}} = \sum_i y_i C_{p_i} \\ y_i = \frac{\rho_i}{\rho_{mix}} \end{cases} \longrightarrow \gamma_{mix} = \frac{C_{p_{mix}}}{C_{p_{mix}} - R_{mix}} \quad (3)$$

where y_i is the mass fraction of species i . As R_{air} has already been computed, only the specific heat at constant pressure $C_{p_{mix}}$ has to be determined. Reminding that the ratio between number density and Avogadro constant is the number of mole per unit volume, the mass density ρ_i of species can be computed as follows:

$$\rho_i = \frac{m_i}{V} = \frac{n_i}{V} W_i = \frac{nd_i}{N_a} W_i \quad (4)$$

where W_i is the molar mass of the species (kg/mol). Mass ratio can be easily computed starting from the number density and the tabulated molar mass of the gas. On the other side the specific heat at constant pressure of species i (C_{p_i}) computation implies more problems because it is a function of temperature and no exact expression exist: NASA report (3) suggests some empirical formulas for species such as N, O, N_2, O_2 and O^+ , while for He, H and Ar , C_{p_i} is constant in the whole range of temperature of interest and it is possible to rely in tabulated value in (4).

2.2 Aerodynamic model

The model proposed by the CNES is inspired by the Newtonian modified method for hypersonic flows (5). The model relies on the hypothesis that, at hypersonic velocities, shock wave lies so close to the surface that it is possible to assume that there is no boundary layer: incoming flow is directly impacting on the wedge surface and then it runs parallel to the surface downstream. According to this theory, the object is seen by the flow as it would have been seen by a parallel beam of light directed as aerodynamic velocity ($\vec{V}_{aero} = \vec{V}_{COG} - \vec{V}_{atm} - \vec{V}_{wind}$, where \vec{V}_{COG} is the velocity of spacecraft (S/C) centre of gravity (CoG), \vec{V}_{atm} is atmospheric velocity computed by taking the cross product between angular velocity of Earth rotation motion and the S/C position in the inertial frame, \vec{V}_{wind} and is wind velocity).

According to Newtonian model, the expression of forces acting on a surface A subjected to a flow characterized by a density ρ_∞ and a velocity V_∞ , ($V_\infty = |\vec{V}_{aero}|$) hitting the surface with an angle θ is:

$$\vec{R} = -\frac{1}{2} \rho_\infty V_\infty^2 A \begin{cases} C_n \cos^2 \theta \vec{n} \\ C_t \cos \theta \sin \theta \vec{t} \end{cases} \quad (5)$$

where \vec{n} and \vec{t} are respectively the normal and tangent vectors, $\theta = \arccos((\vec{n} \cdot \vec{V}_{aero})/|\vec{V}_{aero}|)$, and C_n and C_t are coefficients depending on the type of flow. In fact, a re-entering satellite during its trajectory experiences three different regimes, the continuum regime, the free molecular regime and the transitional one. The parameter that governs the passage between these different regimes is the number of Knudsen K_n , which is the ratio between the mean free path (λ) and the characteristic length of the body subjected to the flow (L). Knudsen number can be computed as follows:

$$K_n = \frac{\lambda}{L} = \frac{k_b T_\infty}{\sqrt{2} \pi d^2 P_\infty} \frac{1}{L} \quad (6)$$

where k_b is the constant of Boltzmann ($1.380622 \cdot 10^{-23}$ J/K), T_∞ and P_∞ are static temperature and pressure of the flow, and d is the average collision diameter of the particles ($3.65 \cdot 10^{-10}$ m).

Even if the Knudsen number depends on the geometry of the spacecraft, an approximate relation between this number and the flight altitude can be established:

$$\begin{cases} K_n < 0.01 & \text{continuum regime} \\ 0.01 < K_n < 10 & \text{transition regime} \\ K_n > 10 & \text{free molecular regime} \end{cases} \longrightarrow \begin{cases} h < 85 \text{ km} \\ 85 \text{ km} < h < 130 \text{ km} \\ h > 130 \text{ km} \end{cases} \quad (7)$$

In continuum flow, C_t is equal to 0 and C_n is equal to $C_{p_{max}}$, the pressure coefficient evaluated at the stagnation point behind a normal shock wave. This value depends on the Mach number M_∞ of the flow and can be computed as follows:

$$C_{p_{max}} = \frac{P_{02} - P_\infty}{\frac{1}{2} \rho_\infty V_\infty^2} = \left(\frac{P_{02}}{P_\infty} - 1 \right) \frac{P_\infty}{\frac{1}{2} \rho_\infty V_\infty^2} = \left(\frac{P_{02}}{P_\infty} - 1 \right) \frac{2}{\gamma M_\infty^2} \quad (8)$$

where P_{02} is the total pressure after the shock and P_∞ is the infinite static pressure. The ratio P_{02}/P_∞ can be computed knowing the jump between infinite static pressure amount the shock and static pressure after the shock (P_2/P_∞) and the relation between total and static pressure downstream (P_2/P_{02}), leading to this formula:

$$C_{p_{max}} = \frac{2}{\gamma M_\infty^2} \left(\left(\frac{(\gamma+1)M_\infty^2}{4\gamma M_\infty^2 - 2(\gamma-1)} \right)^{\frac{\gamma}{\gamma-1}} \left(1 + \frac{2\gamma}{\gamma+1} (M_\infty^2 - 1) \right) - 1 \right) \quad (9)$$

For the friction and the pressure coefficient in the free molecular regime, the CNES propose the empiric values $C_n^{free} = 2.3$ and $C_t^{free} = 1.7$, while in the transition region the coefficient will be computed as an interpolation between the boundary values of coefficients.

For an object made of more than one surface, only the enlightened/not-masked surfaces contribute to the resultants. For an object having N surfaces the expression of aerodynamic forces is:

$$\begin{cases} \bar{F}_n = -\frac{1}{2} \rho_\infty V_{aero}^2 C_n \sum_{i=1}^N \cos^2 \theta_i A_i \bar{\mathbf{n}}_i \\ \bar{F}_t = -\frac{1}{2} \rho_\infty V_{aero}^2 C_t \sum_{i=1}^N \sin \theta_i \cos \theta_i A_i \bar{\mathbf{t}}_i \end{cases} \quad (10)$$

$$\bar{F}_{aero} = \bar{F}_n + \bar{F}_t \quad (11)$$

where $\bar{\mathbf{n}}_i$ is the vector normal to surface i , and is set to zero for all the surfaces i not satisfying the visibility condition ($\bar{\mathbf{n}}_i \cdot \bar{\mathbf{V}}_{aero} > 0$). $\bar{\mathbf{t}}_i$ is the tangent vector to the surface i , in the plane identified by aerodynamic velocity and normal ($\bar{\mathbf{n}}_i \times ((\bar{\mathbf{V}}_{aero} \times \bar{\mathbf{n}}_i) / |\bar{\mathbf{V}}_{aero} \times \bar{\mathbf{n}}_i|)$), A_i is the enlightened area, $\theta_i = \text{acos}((\bar{\mathbf{n}}_i \cdot \bar{\mathbf{V}}_{aero}) / |\bar{\mathbf{V}}_{aero}|)$ is the angle between the velocity and the normal to surface i . Moreover, calling \bar{b}_i the coordinates of the centre of pressure of the surface i with respect to the position of the CoG, it is possible to define:

$$\bar{f}_i = -\frac{1}{2} \rho_\infty V_{aero}^2 (C_t \sin \theta_i \cos \theta_i A_i \bar{\mathbf{t}}_i + C_n \cos^2 \theta_i A_i \bar{\mathbf{n}}_i) \quad (12)$$

so that the aerodynamic torques \bar{T}_{aero} can be computed as follows:

$$\bar{T}_{aero} = \sum_{i=1}^N \bar{b}_i \times \bar{f}_i \quad (13)$$

The need was therefore to develop a tool that, given the aerodynamic angles (which identify aerodynamic velocity direction in S/C reference frame) and a certain geometry, computes for each surface: the visible area, the tangential and normal vectors, the angle θ , and the position of the center of pressure. However, the resulting masking algorithm is relatively slow and could not be used online during the simulations. To overcome this issue, it has been decided to compute offline, for a given geometry, a two-dimensional table that, for each couple of aerodynamics angles, collects the value of aerodynamic forces and torques computed by the masking algorithm. During the simulation, the tool reads the values corresponding to the current couple of aerodynamic angles and performs a bilinear interpolation for those couples of aerodynamic angles that are not tabulated.

2.3 Thermal Model

One of the most constraining factors during an atmospheric reentry is the temperature reached by the solar array. It is therefore out of the scope of the study to determine the temperature evolution for each surface of the spacecraft. The interest is focused only on the side of the solar array covered by the solar cells, because they are subjected to the most restraining temperature limitation and once damaged prevent the production of electric power. A detailed thermal model would include radiative and conductive coupling between solar array and other surfaces, which has been avoided in this preliminary study. Being the typical temperature difference between the front and the back side of the panel around 10 degree, relatively small for the purpose of the thermal analysis to be conducted, a single-node model, which assumes that the temperature is uniform throughout the solar panel thickness, is used. The equation governing the evolution of the solar array temperature T is therefore:

$$\frac{m C}{S_{ref}} \frac{dT}{dt} = \phi_{aero} + \phi_S + \phi_{IR} + \phi_A - \phi_I \quad (14)$$

In the above formula, C is the heat capacity of the panel. It has been taken equal to 830 J/kg/K which is a typical value adopted for solar array design and it is considered to be constant, even in presence of temperature variation. m/S_{ref} is the mass per unit surface of the solar array that is calculated considering a density of 90 kg/m³ for a 3 cm thick array. ϕ_I is the radiative flux exiting the panel due to its temperature. It is equal to $\epsilon\sigma T^4$, where ϵ is the thermal emissivity of the panel and σ the Stefan-Boltzmann constant (5.67 10⁻⁸ W/m²K⁴). ϕ_S is Solar radiative incoming flux, ϕ_{IR} is Earth infrared incoming flux, ϕ_A is the Earth albedo incoming flux. The computation of ϕ_{IR} , ϕ_A and ϕ_S passes from the computation of the view factor for a flat plate. ϕ_{aero} is the flux due to the forced convection caused by the airflow during the atmosphere passages. In the free molecular regime it can be assumed that the molecules that impact the surfaces transfer all their kinetic energy to the hit surface. As flow regime is hypersonic, the static temperature can be neglected with respect to the total one, so that the total enthalpy of the flow (h_0) can be written as follows

$$h_0 = \dot{m} C_p T \left(1 + \frac{\gamma+1}{2} M^2\right) \sim \dot{m} C_p T \frac{\gamma-1}{2} M^2 \quad (15)$$

Being $C_p = \frac{\gamma R}{\gamma-1}$ (C_p specific heat at constant pressure, γ heat capacity ratio, R specific gas constant) and $M = \frac{u}{c}$, where u is the aerodynamic velocity and $c = \sqrt{\gamma RT}$ the speed of sound, it is possible to write:

$$h_0 \sim \dot{m} \frac{\gamma R}{\gamma-1} T \frac{\gamma+1}{2} \frac{u^2}{\gamma RT} = \dot{m} \frac{1}{2} u^2 \quad (16)$$

The mass rate can be written as $\dot{m} = \rho u A \cos\theta$, where θ is the angle between the flow direction and the normal to the visible surface A (see section 2.2). Therefore, the convective heat flow due to the aerodynamic interaction will be:

$$\phi \sim \frac{1}{2} \rho u^3 A \cos\theta C_H \quad (17)$$

where C_H is a corrective coefficient that can be considered equal to 1 for the free molecular flow and gets smaller as the continuum regime approaches. In fact when the density increases, a shock progressively builds up in front of the spacecraft, lowering the energy of the molecules hitting the surfaces. Taking C_H always equal to 1 is therefore a conservative assumption. For each surface of the panel the quantity $A \cos\theta$ is computed by the masking algorithm. This quantity, being the thermal balance equation normalized by the reference area of a solar panel face, has to be divided by the reference surface. The aerodynamic heat flow is therefore:

$$\phi_{aero} = \frac{1}{2} \rho u^3 \frac{A}{S_{ref}} \cos\theta C_H \quad (18)$$

3. Semi-controlled reentry: feasibility study

SWOT (Surface Water and Ocean Topography), the first satellite that will perform a controlled reentry, has been chosen as a test case for a hypothetical electric propelled semi-controlled reentry. SWOT is a French-US mission aimed at carrying out the first global survey of Earth's surface water. The launch is planned for April 16, 2021, and its nominal life will be 3 years, on a circular orbit at 891 km of altitude and 77.6 deg of inclination. The reentry phase is planned to occur in autumn 2025. There will be a series of seven maneuvers that will lower the perigee down to 250 km, and a last burn maneuver that will bring the perigee down to 10 km, causing the reentry of the satellite. The ΔV involved is in the order of 137 m/s for the 7 perigee lowering maneuvers and of 70 m/s for the final burn. To provide this high level of thrust, 8 hydrazine thrusters will be employed (each one providing 22 N of thrust, with an average specific impulse of 221 s). For the purpose of the following test case, the semi-controlled reentry of SWOT is assumed to happen using an electric propulsion system. Electric propulsion main difference with respect to chemical propulsion is the higher specific impulse I_{sp} (about 6 times greater), at the price of a much lower level of thrust. The feeble level of thrust of an electric engine implies that the maneuver can no longer be considered as impulsive: in order to have the same ΔV of a chemical propulsion system, the electric engine shall operate for a longer time. This means that, if on the one hand the high I_{sp} implies savings in propellant consumption (and therefore in the cost of the launch), the duration of the reentry can lead to high ground operation cost.

In order to study the feasibility of the reentry some assumptions on the adopted electrical propulsion system have to be introduced: the chosen propeller is the Hall Effect Xenon propeller PPS 5000, a SNECMA propeller selected by ESA, Thales Alenia Space and Airbus Defense and Space for the NeoSat program. The specific impulse I_{sp} is 1770 s, the thrust 0.303 N, the power consumption 5kW and the average propellant consumption is 1.737 10⁻⁵ kg/s. In this preliminary study, the saving in terms of propellant mass that will be obtained by realizing all SWOT nominal mission with electric propulsion will be computed. The total ΔV of SWOT mission is 322 m/s, including 182 m/s for the perigee lowering phase and 82 m/s for the last burn, which translates, for the nominal chemically propelled mission, in 349 kg

of hydrazine (including 199.4 kg for perigee lowering and 83.6 for the last burn). By applying the Tsiolkovsky law having as input the dry mass of the S/C (~ 2050 kg), the total ΔV of the mission and the I_{sp} of the electric propellant, it is possible to compute the mass of Xenon that is needed on board in order to accomplish the mission, which results in 40 kg for the entire mission, including almost 22 kg for the perigee lowering phase and almost 10 kg for the last burn.

$$\Delta V = I_{sp} g_0 \log\left(\frac{m_i}{m_i + m_{Xe}}\right) \longrightarrow m_{Xe} = m_i \left(e^{\frac{\Delta V}{I_{sp} g_0}} - 1 \right) \sim 40 \text{ kg} \quad (19)$$

This means that the change from chemical to electric propulsion implies a mass reduction of more than 300 kg. Moreover semi-controlled reentry strategy relies on the exploitation of atmospheric drag to decrease the semi major axis. Consequently, the last burn could eventually be avoided. In this latter case, the propellant consumption to accomplish the mission would be around 30 kg of Xenon.

Based on a mere consideration on the mass saving obtained with electric propulsion, it is possible to preliminary asses the average saving in terms of launch price: considering a price of 10000-15000 € per kg at launch, a reduction of 300 kg would imply an saving of the order of 3 to 4.5 million €. On the other side, electric propulsion has not only an outgrowth in terms of S/C design, but also in the duration of the deorbiting: operational cost for the ground segment is about 400 k€ per month and there is necessarily a breakeven point between the two strategies. The aim at this point is to make preliminary evaluation of the ΔT , the number of propeller needed, the power balance when the propeller is functioning (it should be kept in mind that the electric power demand is 5kW) and so on.

3.1 Non impulsive maneuver

Since the maneuvers are not impulsive, the propagation of the orbital elements needs to be studied by including the thrust in the perturbations. To this aim Gauss Equation, written in the orbital reference frame t, n, h (where t is the vector tangent to the orbit -therefore directed as the velocity-, h is the vector normal to orbital plane and $n = h \times t$), are used. During a reentry, the effect that needs to be maximized is the negative variation of the semi-major axis, which means that only a negative tangential thrust should be provided by the propeller. Assuming therefore that only the tangential component of perturbing acceleration f_t is present, the following equations are obtained:

$$\begin{cases} \frac{da}{dt} = \frac{2a^2}{\mu} V f_t \\ \frac{de}{dt} = \frac{2}{v} (e + \cos v) f_t \\ \frac{d\omega}{dt} = \frac{2 \sin v}{e v} f_t \end{cases} \quad (20)$$

f_t has a secular effect on the semi-major axis, a periodic effect on the argument of periapsis, and both secular and periodic effect on eccentricity. Being f_t negative, the semi major axis will decrease regardless the position in which the thrust is applied and there will be eccentricity augmentation (and therefore perigee decrease) for $|v| \in [\arccos(e), \pi]$ ("apogee side" of the orbit, where v is the true anomaly). On the other side, it must be taken into account that, if the aim is to reduce the perigee altitude, eccentricity must be increased. Moreover, assuming to apply the thrust "symmetrically" around the apogee, a null effect on the argument of periapsis (ω) is obtained. The idea of a continuous thrust that would lead the S/C to spiraling down on circular orbits is not taken into account for two reasons: the first linked to the power balance and the other due to the thermal requirements (below a certain altitude the satellite will be continuously subjected to aerodynamic flow and solar array would be compromised). The duration of the maneuver is strictly linked to the power balance. SWOT has a total solar array surface A of $2 \times 2.64 \times 5.9444 = 31 \text{ m}^2$ and the generated power can be computed as follows:

$$P = 0.25 \phi_0 | \cos \delta | A = 10594 \text{ W} | \cos \delta | \sim 10 \text{ kW} | \cos \delta | \quad (21)$$

where δ is the angle between the normal to the solar array surface and the S/C-Sun vector, and $\phi_0 = 1367 \text{ W/m}^2$ is the mean solar flux. This means that, being 5 kW the power consumed by the propeller, only for solar array angles δ from 0 deg to 60 deg (and 120 deg to 180 deg) the produced power will be sufficient to feed the electric propeller. Moreover eclipses period and the AOCS and telecommunication power need are not taken into account. Consequently only a single propeller configuration is possible, and thrust should be applied only for a small percentage of the orbital period. Being v the true anomaly, thrust law can be expressed as follows:

$$\begin{cases} f_t = 0 & 0 \leq |v| \leq \bar{v} \\ f_t = -1.443 \cdot 10^{-4} \frac{m}{s^2} & \bar{v} \leq |v| \leq 180 \text{ deg} \end{cases} \quad (22)$$

The acceleration f_t is computed assuming a single thruster having a thrust of 0.303 N, and an End Of Life mass of 2100 kg (2050 kg of dry mass + 50 kg of propellant margin): $f_t = 0.303/2100 = -1.443 \cdot 10^{-4} \text{ m/s}^2$. \bar{v} is the unknown

true anomaly -determining where thrust period starts- that needs to be optimized. In order to reduce the computational time of each simulation, a version of the simulator that propagates only the translational dynamic has been developed. This version propagates the orbital parameters through Gauss equations and takes into account as perturbation only thrust and atmospheric drag, which are modeled as follows:

$$f_d = -\frac{1}{2}V^2\rho \frac{(A C_D)}{m_{sat}} \quad (23)$$

where $A C_D$ (which is the product of the exposed surface and the drag coefficient) is computed numerically thanks to the masking code (using the coefficient of free molecular flow and the exposed area in SWOT reentry attitude) and is equal to 20.9 m². The simulator computes the evolution of the orbital parameters from the nominal orbit to the moment where perigee altitude reaches 250 km for different values of $\bar{\nu}$, providing as outputs both the duration of the maneuver and the initial conditions for a full 6-DoF simulation with the main simulator. For the values of $\bar{\nu}$ equals to 150 deg, 140 deg, 135 deg, the perigee altitude of 250 km is reached respectively after 81.4 days, 62.5 days and 56.3 days, at an apogee altitude of 868 km, 857 km and 850 km respectively. Since there are no appreciable differences either in the apogee altitude or in the consumed propellant (which is mainly related to the variation of semi-major axis), the shorter maneuver should be preferable ($\bar{\nu}$ =135 deg), but the compatibility with the power balance has to be studied. It has to be kept in mind that the nominal attitude of SWOT during reentry implies a fixed orientation of the SA, with the normal to the surface lying in the orbital plane (therefore orthogonal to the angular momentum). As panels cannot be orientated towards Sun, when studying the feasibility of the maneuver, the energy balance needs to be analyzed for the entire domain of possible relative angle between Sun and the orbital plane ($\bar{\Omega}$), whose value is a combination of the simulation date and the RAAN. Assuming, for this preliminary study, that the apparent movement of Sun is on the equatorial plane (declination always equal to 0 deg), the exposition can be studied by keeping fixed the date and changing only the value of Ω , that will now be a relative Sun/orbital plane angle. The presence of J_2 perturbation will contribute to the variation of Ω and ω which have a direct influence on the exposition of solar panel.

3.2 Power balance during perigee lowering phase

This chapter deals with the power balance during the perigee lowering phase. In section 3.1 it is shown that relatively long periods of time have to be taken into account in order to reach deorbiting. During this period orbital parameters cannot be considered constant. The presence of J_2 perturbation will contribute to the variation of Ω and ω which have a direct influence on the exposition of solar panel. While Ω has a direct influence on the solar angle δ , ω affects the position of the eclipse period on the orbit. Of course, the optimal condition would have the perigee placed in eclipse in order to perform thrust during the daylight period. By averaging the initial nominal orbit and the final orbit after the perigee lowering phase, Ω will vary with an angular speed of -1.5 deg/day, to which it has to be added the variation due to the rotation of the Earth around Sun, resulting in an average angular speed of -2.5 deg/day, and ω with an angular speed of 3 deg/day. To be feasible, the power balance during the whole maneuver duration must be positive for all the range of Ω and ω . The power need is not constant within one orbit. As already said, electric propeller will consume 5kW when functioning. The value for the AOCS power need has been fixed considering 4 reaction wheels (30 Nms max momentum, 0.215 Nm max torque), with a maximum consumption (at max Torque) of 150 W each (600W for all the wheels) and 3 magnetorquers (6.5 W x 3). The value of 1 kW has been fixed to be conservative. For the following simulations, thrust will be “on” for true anomalies $|\nu| \in [\bar{\nu}, 180 \text{ deg}]$, and the AOCS will be considered as functioning at its maximum performance below 300 km of altitude. The battery will be a 250 Ah battery providing a routine voltage of around 30 V, resulting in a capacity of 7500 Wh (27 000 kJ). Using these inputs the power balance is analyzed for each choice of $\bar{\nu}$ for all couples of Ω and ω , and the result is that the choice of $\bar{\nu} = 150 \text{ deg}$ seems to be the most promising. In fact simulations show that the power balance is negative over one orbit only for a small range of Ω that goes from 82.5 deg to 97.5 deg (or 262.5 deg to 277.5 deg), therefore a range of 15 deg. In this angular range, due to the combination of satellite altitude and inclination, when the orbital nodal line is almost orthogonal to Sun, the satellite is always illuminated. Even if the satellite never goes in eclipse, the angle between solar arrays and Sun prevents the production of the needed energy (this is comprehensible considering that the solar panel normal is almost orthogonal to the Sun-Earth direction since it lies in the orbital plane). A range of 15 deg corresponds to almost six days (considering a $\Delta\Omega$ per day of -2.5 deg) during which it will not be possible to perform the thrust, which is a small percentage of time with respect to the whole duration of the maneuver (that will be around 3 months). If it is not desired to increase the duration of the whole maneuver, it is possible to assume starting the maneuver in a favorable configuration in terms of exposition, in order to increase the thrust duration during the initial phase (where satellite is above 300 km and AOCS power need is negligible). So, assuming to set $\bar{\nu} = 150 \text{ deg}$ (which corresponds to thrusting for the 17.4% of the orbital period), the duration of the maneuver will be about 3 months, which translates in almost 1.2 million € of ground operation cost, namely the 30% of the amount saved in launching phase. During the perigee lowering phase apogee and perigee altitude will assume the shape reported in Fig. 3:

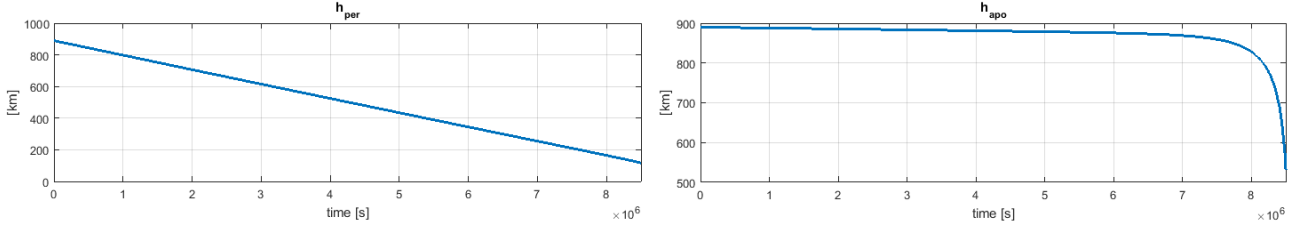


Figure 3: perigee (h_{per}) and apogee (h_{apo}) altitude evolution during reentry

The perigee (left figure) keeps decreasing almost linearly due to the propulsion in apogee that gives a ΔV almost constant within the whole duration, while apogee (right figure) is almost constant and start decreasing exponentially as the perigee reaches 250 km. This can be explained by equaling the ΔV provided by the thrust to the one provided by the aerodynamic drag. In the left side of the following equation there is the effect of propulsion within one orbit, and on the right side drag effect, assuming that it acts for almost one half of the orbital period:

$$\Delta V_{thrust} = f_t \times \Delta T_{thrust} = \Delta V_{drag} = \frac{1}{2} V^2 \rho \frac{(A C_D)}{m_{sat}} \times \Delta T_{drag} \longrightarrow \rho = \frac{\Delta V_{thrust} m_{sat}}{\Delta T_{drag} (A C_D) V^2} \sim 10^{-10} \text{ kg/m}^3 \quad (24)$$

The equation is solved for the value of density $\rho \sim 10^{-10} \text{ kg/m}^3$ which corresponds, for a normal solar activity, to the altitude of 250 km, exactly where the apogee lowering rate becomes much faster than perigee lowering rate and starts increasing exponentially (as the density does).

3.3 Decay phase: controllability limits

At this point sustainability of the perigee lowering phase has been demonstrated, and simulations will be refined by fixing a minimal altitude of the perigee that will correspond to the last controllable apogee. SWOT AOCS is designed to be nominally controllable down to 250 km and, being the perigees of the last days of maneuver lower than 250 km, there will be a short arc around the perigee where the satellite is not controllable and starts changing its attitude by tumbling. During the first revolutions the control will be capable to re-find its attitude in order to perform the thrust at apogee. But, as perigee continues to decrease, the rotation rate will become too important and the S/C will become uncontrollable even if the apogee is still above 250 km. The objective is now to identify which are the controllability limits of the satellite and therefore to define the initial conditions of the decay phase. The simulations will be performed on the main simulator, starting from an orbit having perigee at 250 km and apogee at 868 km (output of the lighter version of the simulator for $\bar{v} = 150 \text{ deg}$).

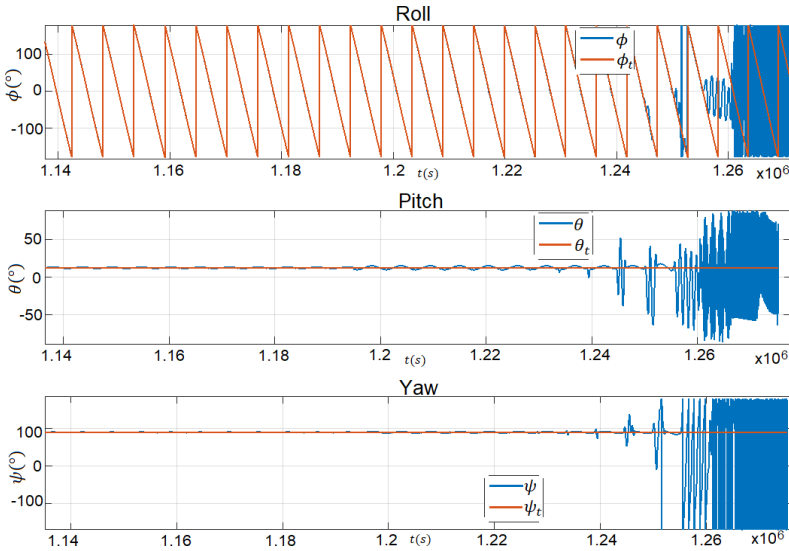


Figure 4: Real and target attitude during last 20 orbits

Figure 4 shows SWOT real and target attitude in the last 20 orbits before the reentry (ϕ, θ, ψ are respectively roll, pitch and yaw angles, and ϕ_t, θ_t, ψ_t the corresponding target angles). Looking at Fig. 4 it can be noticed that the oscillations start diverging for $t > 1.24 \cdot 10^6 \text{ s}$, which corresponds to a perigee altitude of 119 km, but it is actually not possible to define clearly which is the last controllable orbit and the first uncontrolled one. It has been decided therefore to analyze two different cases in order to see which is the influence on compliance with SDM requirements. The two cases will be referred to as corresponding to assuming the S/C controllable until orbit N and N+1, respectively. Orbital parameters in these two cases will be the initial conditions of

two different decay (non-controlled) phases. Being h_p and h_a the perigee and apogee altitude, the initial conditions of case N correspond to $h_p=119.5 \text{ km}$, $h_a=544.4 \text{ km}$, while the initial conditions of case N+1 correspond to $h_a=528.6 \text{ km}$, $h_p=118.7 \text{ km}$. Before proceeding, it is necessary to check if the solar array temperature stays below the 150°C during the entire controlled and propelled phase: if it is not the case, the solar cells of the GS have reached their maximal operational temperature and cannot produce the needed power. However, since the attitude of SWOT during reentry minimizes the surface of GS exposed to the flow, this problem shows up only when the satellite starts tumbling and does not represent an additional constraint in our case. The temperature stays in the range from -60°C to $+80^\circ \text{C}$ for the

overall maneuver, and start diverging only below 118 km ($1.25 \cdot 10^6$ s).

The subsequent simulations answer several questions, such as how many orbits from the end of the control instant are flown before satellite reentry, what is the altitude of last perigee-apogee before reentry, what is the rotation rate of the satellite (if the tumbling rate becomes too high during the decay orbit, satellite can break because of centrifugal force when still in orbit; moreover the increase in rotation rate affects the choice of the integration step) and so on. In particular the focus will be on the ground-tracks of the decay orbits, and in the way to connect the outputs of the simulator to the inputs needed from software that computes satellite fragmentation. In fact the simulator is considered to be valid only above 90-80 km of altitude, which represents a mechanical limit: dynamic pressure below these altitudes becomes too high and causes the fragmentation of the satellite. Figure 5 shows the evolution of altitude in the

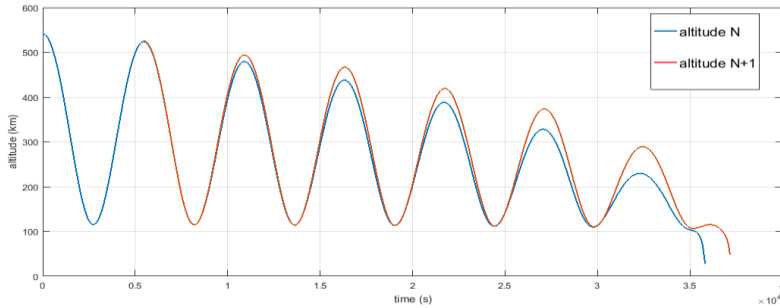


Figure 5: Evolution of altitude in cases N and N+1

two different situations (N, N+1). As it is possible to see, the first reentering satellite is the one that is thrust and controlled for N orbit.

This is a little bit counterintuitive because the satellite that first reenters is the one that undergoes a shorter propelled phase: this is explainable because SWOT tumbling average surface is 50% larger than the controlled one (10m^2 vs 15m^2), so the action of drag during the tumbling perigee

passage is higher than the contribution of thrust during apogee passage: this means that in this last phase anticipating the end of the control phase accelerates the decay phase. More in details, after the first orbit, when N+1 case starts, the perigee of the case N is 118.8km (therefore higher than N+1, which is 118.7km, since the propulsion did not act at apogee), while N apogee is 527.2 km (way lower than apogee of the case N+1, which is 528.6km, and this is due to the higher drag experimented). Concerning rotation rate, at each atmospheric passage, frequency and amplitude of rotation increase, but they increase abruptly only during the last (and reentering) atmospheric passage. Before this passage the rotation rate stays below the 3 rpm, allowing to state that there is no destruction due to centrifugal forces.

3.4 Compliance with SDM requirements

The focus will be now on the satellite ground-tracks. In order to be compliant with the SDM requirements, the risk of casualty has to be lower than 10^{-4} . Since a satellite of SWOT dimensions will not completely burn up during reentry and some debris will surely reach ground, the risk of casualty has to be managed by phasing the maneuver in order to have the last orbit ground-track over the least populated areas. The aim is to find the proper phasing that maximizes the number of ground-tracks not covering populated areas. Once the final ground-track has been fixed, the phasing is translated in an initial epoch and ω .

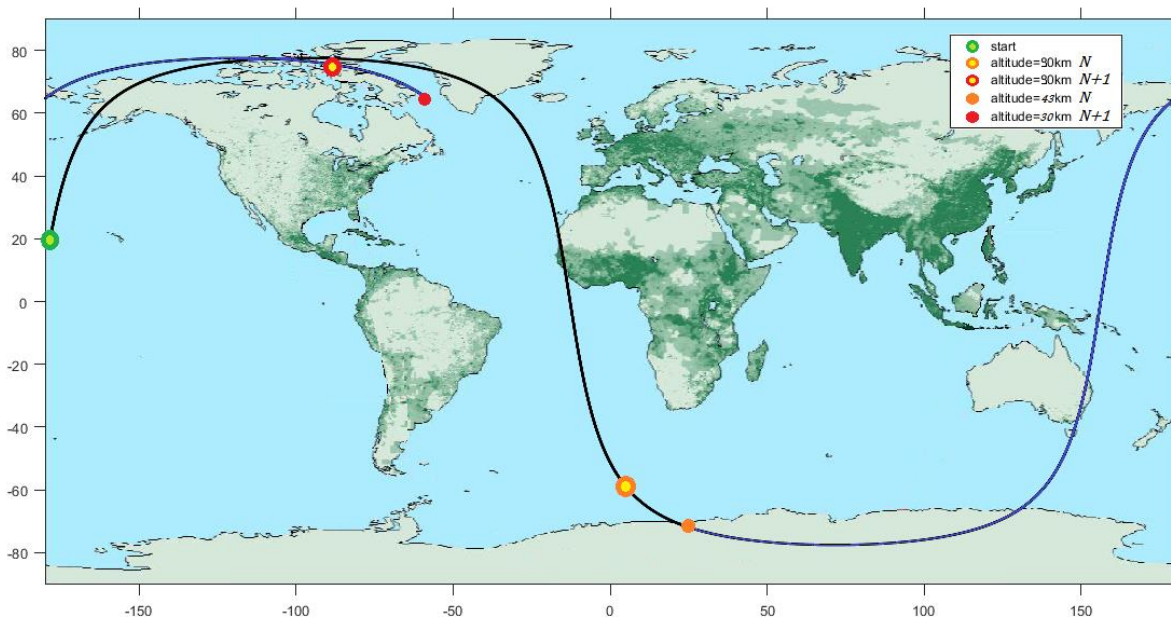


Figure 6: Ground-tracks from last apogee

Figure 6 shows the ground-tracks corresponding to both cases starting from their last apogee (which is almost 290 km for N case and 230 km for N+1): the initial conditions are the orbital parameters corresponding to of the last apogee before reentry (the green point in Fig. 6 with $\omega = -160$ deg at the date of 21/03/2026, 00h 17min 38s). Table 1 shows orbital parameters of both cases taken in correspondence of the last apogee:

	a [km]	e	i [deg]	Ω [deg]	ω [deg]	θ [deg]
N	7000.1	0.01373	77.558	0	-160	-180
$N+I$	6546.6	0.00932	77.573	0	-160	-180

Table 1

The choice of ω is very important: for instance, choosing ω equal to ± 90 deg will place the perigee in correspondence of the poles. Earth radius at the poles is 7 km shorter than at the equator. This means that, when the perigee is placed at the pole, for the same perigee radius r_p the satellite will experiment a higher perigee altitude h_p with respect to a case with perigee placed at equator. A higher geodetic altitude translates in a lower density and therefore a lower drag, which results in a delay in the reentry. This means that, once the feasibility of reentry is studied and the final ground-track chosen, it will be necessary to work backwards in order to loop-back the final conditions (such as date and orbital parameters) with the beginning of the entire semi-controlled reentry phase. In Fig. 6 the green point represents the departing point (apogee), the black ground-track is the trajectory followed in both cases, the blue ground-track is the trajectory followed only in case N+1, yellow-orange point represents the interface a 90 km for the N case, and yellow-red point the 90 km for N+1 case. Orange point (Antarctic) and red point (Greenland) represent respectively the ends of simulation of N and N+1 cases, which happen at 43km and 30 km. It has been said that the results of the simulator are valid only until the fragmentation of the S/C (above 90-80 km), but what happens after fragmentation can still give some interesting information about the relation between altitude loss and covered distance on the surface. Even if it is possible to place both cases on the same ground-track and to intuitively state that the satellite falls in both cases in inhabited areas, the compliance with SDM has to be studied now by computing fatality risk using a software that analyzes S/C fragmentation and the debris falling zone. These simulations are performed using SARA (Survival and Risk Analysis), an ESA tool in DRAMA (Debris Risk Assessment and Mitigation Analysis) package (6). SARA needs, as input, a detailed model of the internal structure of the satellite (object, size, materials), and the initial conditions, which can be given in the form of the 6 classical orbital parameters. The semi major axis and the eccentricity of the initial conditions must correspond to a perigee altitude higher than 0km, which was not the case for yellow points in Fig. 6 (when satellite altitude is equal to 90 km, the perigee of the orbit is already lower than Earth surface). Therefore others interface points that satisfy the constraint on SARA inputs had to be chosen. These points are yellow points in Fig. 7 (left figure) and Fig. 8 (left figure) and both correspond to an altitude of 102 km. The starting epoch of the simulation is computed by adding to the initial date 21/03/2026, 00h 17min 38s, the simulation time in order to reach the point at 102 km. Table 2 shows initial conditions and time corresponding to yellow points (date is always 21/03/2026).

	<i>Start time</i>	a [km]	e	i [deg]	Ω [deg]	ω [deg]	θ [deg]
N	01h 05min 59s	6432	0.007612	77.5517	-0.0085	-17.8956	-159.72
$N+I$	02h 01min 22s	6435	0.008054	77.5376	-0.0097	-138.83	-137.78

Table 2

These initials conditions correspond to geographic coordinates of $(37.124^\circ S, 5.45^\circ W)$ for the N orbit case (Fig. 7) and $(75.91^\circ N, 147.03^\circ W)$ for the N+1 orbit case (Fig. 8).

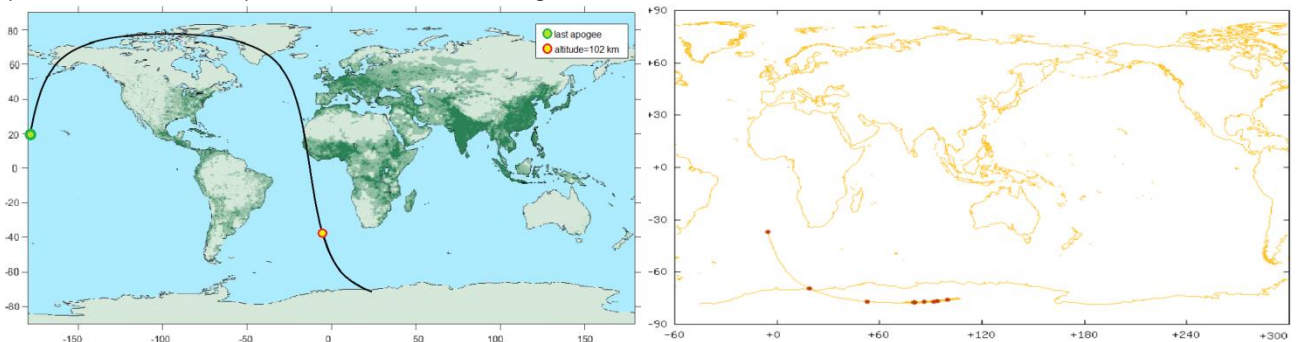


Figure 7: Case N, Simulator interface with SARA

SARA confirms the validity of the results by translating the initial conditions in the same latitude and longitude computed by the simulator. Figure 7 shows the results of SARA simulation for the N case. The first red point in Fig. 7 (on the right), is placed exactly in the same position of the yellow point in Fig. 7 (on the left). In the right figure the footprint of the fragmented debris, which will all fall in the Antarctic, is plotted. The same consideration can be done for the case N+1, in Fig. 8: the red starting point on the right figure, in north of Alaska, corresponds to the yellow point in left figure. The footprint of the fragmented debris is in Labrador sea, between Groenland and Labrador peninsula.

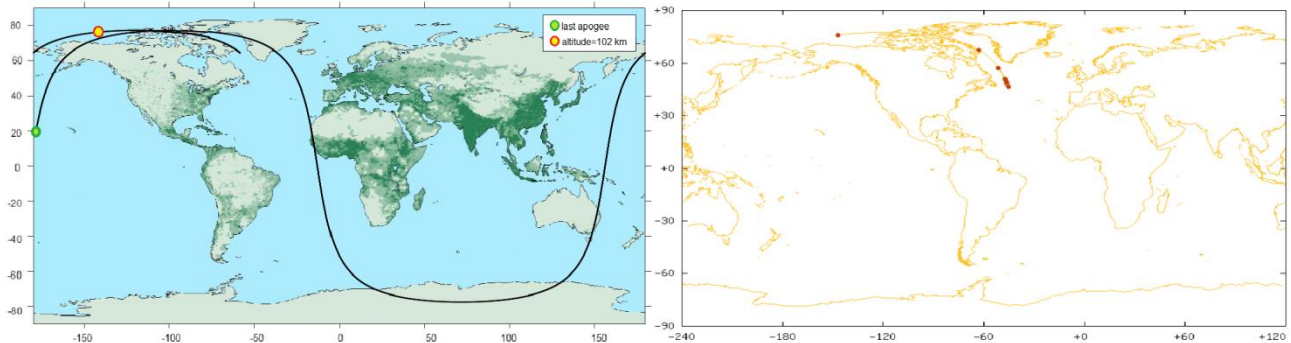


Figure 8: Case N+1, Simulator interface with SARA

In both cases, the casualty risk is lower than 10^{-4} . This means that, even if in presence of an uncertainty in the number of orbits that the satellite is able to control, in both cases the SDM requirements are satisfied, thus implying that, under the hypothesis of this study, the semi-controlled reentry is feasible.

4. Conclusions

This study was aimed to define a strategy for the semi-controlled reentry of a satellite and evaluate its feasibility by means of simulations, from the nominal orbit to the impact. The feasibility of the semi-controlled reentry has been discussed in general terms and any future feasibility study should be adapted to the specific mission (specific platform, power system, AOCS, nominal orbit). The feasibility of the semi-controlled reentry could be adopted in future work to guide the design of the satellite by supporting the selection of the reaction wheels to ensure controllability down to a certain altitude, or by suggesting larger solar arrays to guarantee the power needed by the electric thruster. Future work will address the propagation of uncertainties on the atmospheric model (density and wind), as well as those in the force model (aerodynamic coefficients, error linked to the Newtonian model). In particular their impact on the duration of deorbiting and the total length of the possible footprint should be analysed to understand whether the parallel contribution of all disturbances would still ensure a maximal footprint length of 1-2 ground-tracks that the compliance with SDM.

5. Acknowledgment

I would like to thank Brice Dellandrea and Gautier Durand, who provided me with all the means to carry out this study, and Pierluigi Di Lizia, who helped me enhance my work from an academic point of view.

Bibliography

- ¹ Liou, J. C., et al., "Stability of the future LEO environment – an IADC comparison study", *Proceedings of the 6th European Conference on Space Debris*, Vol. 723, 2013.
- ² European Commission for Space Standardisation, "Space environment", 31 July 2008, ECSS-E-ST-10-04C
- ³ Gupta, Roop N., et al., "A review of reaction rates and thermodynamic and transport properties for an 11-species air model for chemical and thermal nonequilibrium calculations to 30000 K." NASA-RP-1232, 1990.
- ⁴ Ehlers, Janet G., et al., "Thermodynamic properties to 6000 K for 210 substances involving the first 18 elements", NASA-SP-2001, 1963.
- ⁵ Anderson, J. D., *Hypersonic and high temperature gas dynamics*, AIAA, 2000.
- ⁶ Martin, C., et al., "Debris Risk Assessment and Mitigation Analysis (DRAMA) Tool.", Final Report ESA Contract 16966/02, 2005